PERGAMON

International Journal of Heat and Mass Transfer 44 (2001) 2493–2504

International Journal of HEAT and MASS TRANSFER

www.elsevier.com/locate/ijhmt

Analysis of flow and heat transfer in a regenerator mesh using a non-Darcy thermally non-equilibrium model

K. Muralidhar [1], K. Suzuki *

Department of Mechanical Engineering, Kyoto University, Yoshidahonmachi, Sakyo-ku, Kyoto 606-8501, Japan

Received 11 March 1999; received in revised form 3 August 2000

Abstract

An analysis has been made for the pulsating flow of gas and the accompanying heat transfer within a regenerator made from mesh screens. A flow model is developed taking the mesh as a non-Darcy, thermally non-equilibrium porous medium. A harmonic analysis technique is used for solving the fully developed but unsteady gas flow in the regenerator. Based on the flow solution thus obtained, slowly evolving axisymmetric unsteady thermal fields are solved numerically over a wide range of frequencies by making use of the finite volume method. Presentation is made of the friction factor and regenerator effectiveness. Effects of Reynolds number and frequency on the temperature profile and the transient behavior of the system are discussed. The importance of a thermal time constant of the system and length-to-radius ratio of the regenerator demonstrated.

1. Introduction

Metallic meshes are now widely employed in heat transfer applications, for example as regenerators in Stirling cryocoolers [1,2], in waste heat recovery units of gas turbines and in the enhancement of cooling of electrical and electronic equipments [3]. The present study deals with the flow and related heat transfer within the mesh-type regenerators, particularly for the ones to be used in the Stirling cycle devices. Stirling cycle attains the Carnot efficiency under ideal conditions. However, it is not actually attained owing to imperfections in components, particularly by those of regenerators. Most published models treat the regenerators as perfect [4,5]. For instances, pressure drop is neglected, transverse temperature distribution is assumed to be uniform and the streamwise temperature distribution is linear (sometimes constant) and time independent. Clearly these are only approximately attained and should be affected by various parameters like the Reynolds number, pulsating frequency, thermal properties both of gas and mesh, and mesh structure. Therefore, it is certainly important to see how each parameter affects the flow and thermal performance of regenerators. To the authors' knowledge, only a few detailed studies on regenerators have so far [6–8] been published. The present study was initiated to clarify how the above-mentioned parameters are related to the performance of regenerators. In this article, a numerical study will be carried out employing an approach to treat the mesh as a porous medium. Porosity and permeability are used to characterize the geometry of the mesh. Permeability is determined so as to match the friction factor data obtained from steady flow experiments. The extended form of Darcy law to take account of the presence of solid wall, inertia and viscous effects, and vortex formation in pores has been utilized [9]. Interesting studies taking account of such non-Darcy effects have been reported by many researchers including Vafai and Kim [10], Lauriat and Prasad [11], Lage [12], and Antohe and Lage [13] for various problems. In the present study, the non-Darcy treatment of [14] is adopted. One assumption often adopted in the published literature is the thermal equilibrium between fluid in pores and solid material of the porous medium. For

* Corresponding author. Tel.: +81-75-753-5250; fax: +81-75-753-5851.

E-mail address: ksuzuki@mech.kyoto-u.ac.jp (K. Suzuki).

[1] On leave from Indian Institute of Technology, Kanpur 208016, India.

0017-9310/01/$ - see front matter
PII: S0017-9310(00)00285-4

Nomenclature

A_{IF}	specific area of the porous insert: $4(1-\varepsilon)/d_w$ (m^{-1})
A_F	non-dimensional value of A_{IF} : $A_{IF}R$
Bi	apparent Biot number: hR/k_s
d_h	hydraulic diameter of the porous insert: $\varepsilon d_w/(1-\varepsilon)$ (m)
d_w	mesh wire diameter (m)
Da	Darcy number: K/R^2
E	regenerator effectiveness: Eq. (34)
F_ε	Ergun coefficient
f_j	jth harmonic of friction factor equal to $\lvert P_j\rvert$
f_{eq}	total equivalent friction coefficient: Eq. (32)
h	overall heat transfer coefficient between the regenerator and the ambience (W/m^2 K)
k	thermal conductivity (W/m K)
K	permeability (m^2)
Nu	Nusselt number
p	non-dimensional fluid pressure scaled with ρW^2
P_j	non-dimensional pressure gradient for jth harmonic scaled with $\rho W^2/R$
Pr	Prandtl number
r	non-dimensional radial coordinate scaled with R
R	tube radius (m)
t	non-dimensional time scaled with (R/W)
T	temperature (K)
w	non-dimensional axial velocity scaled with W
W	velocity amplitude of pulsating flow (m/s)
$\overline{w}$	cross-sectional mean velocity scaled with W
z	non-dimensional axial distance scaled with R
α_f	thermal diffusivity of the fluid (m^2/s)
β	fluid-to-solid specific heat ratio
Γ	fluid-to-solid effective thermal conductivity ratio
ΔT	reference temperature difference: $T_H - T_L$ (K)
λ	fluid-to-solid thermal conductivity ratio
ε	porosity
ϕ_j	non-dimensional velocity amplitude of jth harmonic scaled with W
μ	viscosity (Pa s)
ρ	fluid density (kg/m^3)
θ	non-dimensional temperature: $(T-T_L)/\Delta T$
τ_c	thermal time constant of the porous insert (s)
ω	pulsating frequency of the flow scaled with ω_c
ω_c	characteristic frequency: π/τ_c (s^{-1})

Subscripts

f	fluid phase
H	hot half cycle
j	jth harmonic
L	cold half cycle
R	quantity scaled with R as the length scale
w	quantity scaled with d_w as the length scale
s	solid phase

instance, Sozen and Kuzay [15] have studied heat transfer in a tube enhanced with mesh screens by making use of thermal equilibrium approximation. Kim et al. [16] have studied heat transfer in a channel filled with porous material subjected to oscillatory flow with non-Darcy approach but with the equilibrium assumption for thermal fields. Thermal performance of regenerators totally depends on heat transfer between fluid and solid phases. Therefore, individual phase should have a temperature difference from another. This is thermal non-equilibrium. Actually, in the studies of Kuznetsov [17,18] on packed beds, phase difference was suggested to occur between the propagating waves in fluid phase and solid phase due to the effects of thermal non-equilibrium. In the works of Kuznetsov and Vafai [19] on packed bed and Vafai and Sozen [20] on porous bed, effects of non-equilibrium were suggested to be more significant at higher Reynolds number and for higher porosity. High velocity and high porosity are the conditions that are often encountered in regenerators. Therefore, adoption of thermal non-equilibrium approach is crucial in the study of thermal performance of regenerators.

2. Mathematical model

2.1. Numerical procedures

The numerical computation will be carried out for flow and temperature fields inside a porous insert, the model of a mesh illustrated in Fig. 1, which locally fills a straight tube being subjected to the pulsating flow of incompressible fluid with zero mean velocity. Gas flows into the porous insert through its hot end with a temperature T_H in a hot half cycle and flows back into the insert through its cold end with another lower temperature T_L in a cold half cycle. Although the temperature difference ΔT $(= T_H - T_L)$ is not small in practical

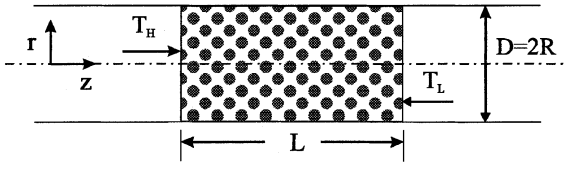

Fig. 1. Physical model and coordinate system.

situation, it is treated to be small in this study just as the first approximation. Gas velocity in practical applications is in the range of 5–10 m/s. So, fluid compressibility due to velocity change is not of primary importance. Effects of density change due to pressure change and temperature non-uniformity may be worth studying but in the present study this will be left as topics for future study. Wall effects are confined in a layer of the order of $R\sqrt{Da}$, where Da is the Darcy number and R is the tube radius [10]. In the present study, $\sqrt{Da}$ is of the order less than 10^{-2}. Therefore, the flow should develop in a short distance inside the porous insert. Thus, the flow is treated to be fully developed and hence fluid velocity to be a function of time and radial position. Thermal field inside the porous insert, on the other hand, is treated as axisymmetric, time-dependent but developing. Thermal field is regarded to attain dynamic steady state much more slowly than the flow field. This is validated by the small value of the ratio between the flow and the thermal field time scales. Numerical results to be obtained will be presented first for the cases equivalent to experiments reported in the references [7,15]. In the calculations, Reynolds number, Re, based on the tube radius, R, and the amplitude of velocity fluctuation, W, is changed from 100 to 10 000. At very high Darcy number or at high porosity, flows can become turbulent at high Reynolds numbers studied in this article. In this paper, the flow instability will be discussed. However, turbulence in porous media will also be left as a topic for future studies. Length-to-radius ratio of the insert is changed from 1 to 20. Non-dimensional flow pulsating frequency ω, i.e., the frequency normalized with the characteristic frequency ω_c defined with the thermal time constant to be shown later, is changed from 1 to 1000. The governing equations to be solved are the mass conservation equation, momentum equation for the fluid phase, and two energy equations both for fluid and solid phases. They may be written in the following non-dimensional forms for the r–z cylindrical coordinate system:

$$\frac{\partial w}{\partial z} = 0, \tag{1}$$

$$\frac{1}{\varepsilon}\frac{\partial w}{\partial t} = -\frac{\partial p}{\partial z} - \frac{1}{Re_R Da} w + \frac{1}{\varepsilon Re_R}\left(\frac{\partial^2 w}{\partial r^2} + \frac{1}{r}\frac{\partial w}{\partial r}\right) - \frac{F_\varepsilon}{\sqrt{Da}} w^2, \tag{2}$$

$$\text{Fluid}: \quad \varepsilon\frac{\partial \theta_f}{\partial t} + w\frac{\partial \theta_f}{\partial z} = \frac{1}{Re_R Pr}\left\{\frac{1}{r}\frac{\partial}{\partial r}\left(r\Gamma_r\frac{\partial \theta_f}{\partial r}\right) + \frac{\partial}{\partial z}\left(\Gamma_z\frac{\partial \theta_f}{\partial z}\right)\right\} - \frac{Nu_R A_F}{Re_R Pr}(\theta_f - \theta_s), \tag{3}$$

$$\text{Solid}: \quad (1-\varepsilon)\frac{\partial \theta_s}{\partial t} = \frac{\beta}{\lambda}\frac{1}{Re_R Pr}(1-\varepsilon)\left\{\frac{\partial^2 \theta_s}{\partial r^2} + \frac{1}{r}\frac{\partial \theta_s}{\partial r} + \frac{\partial^2 \theta_s}{\partial z^2}\right\} + \frac{Nu_R A_F \beta}{Re_R Pr}(\theta_f - \theta_s). \tag{4}$$

The symbols appearing in the above set of equations are as follows: w is the non-dimensional velocity component along the non-dimensional axial coordinate z normalized with the velocity fluctuation amplitude W; r the non-dimensional radial coordinate; θ the non-dimensional temperature which is the difference from the reference temperature T_L and normalized with ΔT; Nu_R the Nusselt number defined with R as the representative length scale; F_ε the Ergun factor; Pe the Peclet number; A_F the non-dimensional specific surface area of the porous insert; ϵ the porosity; β and λ the fluid-to-solid ratios of heat capacity and thermal conductivity; Γ_z and Γ_r the ratio between the effective value and the actual solid property value of thermal conductivity; subscripts f and s are for fluid and solid phases, respectively.

3. Computation of flow field

To solve the momentum equation, a harmonic analysis technique is used. First, the dimensionless cross-sectional mean velocity $\overline{w}$ is assumed to oscillate at a non-dimensional operating frequency ω. Thus,

$$\overline{w(t)} = \exp(i\omega t), \tag{5}$$

where $i = \sqrt{-1}$. The profile of fully developed gas velocity at dynamic steady state is expanded in the following form:

$$w(r,t) = \sum_{j=1}^{N} \phi_j \exp(ij\omega t). \tag{6}$$

In accordance with this, pressure gradient is also expressed as

$$-\frac{dp}{dz} = \sum_{j=1}^{N} P_j \exp(ij\omega t), \tag{7}$$

where ϕ_j is a complex function of r and P_j is a complex constant. In the present study, the number of modes, N, is taken to be 4. Inclusion of higher modes was not necessary in the studied conditions. Substituting these expansions into Eqs. (1) and (2) and collecting terms of each order leads to the following equations:

$$\frac{\partial \phi_j}{\partial z} = 0, \quad j = 1,2,3,4, \tag{8}$$

$$\frac{i\omega}{\varepsilon}\phi_1 = P_1 - \frac{1}{Re_R Da}\phi_1 + \frac{1}{\varepsilon Re_R}\left(\phi_1'' + \frac{1}{r}\phi_1'\right), \tag{9}$$

$$\frac{2i\omega}{\varepsilon}\phi_2 = P_2 - \frac{1}{Re_R Da}\phi_2 - \frac{F_\varepsilon}{\sqrt{Da}}\phi_1^2 + \frac{1}{\varepsilon Re_R}\left(\phi_2'' + \frac{1}{r}\phi_2'\right), \tag{10}$$

$$\frac{3i\omega}{\varepsilon}\phi_3 = P_3 - \frac{1}{Re_R Da}\phi_3 - \frac{2F_\varepsilon}{\sqrt{Da}}\phi_1\phi_2 + \frac{1}{\varepsilon Re_R}\left(\phi_3'' + \frac{1}{r}\phi_3'\right), \tag{11}$$

$$\frac{4i\omega}{\varepsilon}\phi_4 = P_4 - \frac{1}{Re_R Da}\phi_4 - \frac{F_\varepsilon}{\sqrt{Da}}\left(\phi_2^2 + 2\phi_1\phi_3\right) + \frac{1}{\varepsilon Re_R}\left(\phi_4'' + \frac{1}{r}\phi_4'\right), \tag{12}$$

where prime and double primes denote, respectively, the first and second derivatives with respective to r. Coupling between pressure and velocity can be resolved by employing the mass conservation equation

$$\int_0^1 2r\phi_j(r)\,dr = I, \quad j = 1,2,3,4, \tag{13}$$

where I is 1 for $j = 1$ and is zero otherwise. Applying this equation to each of Eqs. (9)–(12), the following algebraic equations can be obtained.

$$\frac{i\omega}{\varepsilon} = P_1 - \frac{1}{Re_R Da} + \frac{2}{\varepsilon Re_R}\phi_1'(1), \tag{14}$$

$$0 = P_2 - \frac{F_\varepsilon}{\pi\sqrt{Da}}\int_0^1 2\pi r\phi_1^2\,dr + \frac{2}{\varepsilon Re_R}\phi_2'(1), \tag{15}$$

$$0 = P_3 - \frac{F_\varepsilon}{\pi\sqrt{Da}}\int_0^1 4\pi r\phi_1\phi_2\,dr + \frac{2}{\varepsilon Re_R}\phi_3'(1), \tag{16}$$

$$0 = P_4 - \frac{F_\varepsilon}{\pi\sqrt{Da}}\int_0^1 2\pi r(\phi_2^2 + 2\phi_1\phi_3)\,dr + \frac{2}{\varepsilon Re_R}\phi_4'(1). \tag{17}$$

Eliminating P_j of Eqs. (9)–(12) with Eqs. (14)–(17), differential equations for ϕ_j are obtained. The boundary conditions to solve Eqs. (8)–(12) are as follows:

$$\phi_j\big|_{r=1} = 0, \tag{18}$$

$$\left.\frac{\partial\phi_j}{\partial r}\right|_{r=0} = 0. \tag{19}$$

The first equation describes the no-slip condition at the wall and the second the axisymmetry of the flow. Separating real and imaginary parts of equations from each other, both the real and imaginary parts of ϕ_j can be determined. However, simultaneous solutions for these are still required in the solution process. This is because the gradient of ϕ_j at the wall appearing in Eqs. (14)–(17) is an unknown complex constant and should be determined simultaneously so as to fit the final solution for ϕ_j. By making use of Newton–Raphson scheme, the real and imaginary parts of ϕ_j have been solved by iteratively correcting the complex velocity gradient at the wall. Once the solution is obtained, pressure field can be calculated from Eqs. (14)–(17).

3.1. Computation of temperature fields

Energy equations (3) and (4) have been discretized with the finite volume method. Central differencing was applied to the diffusion terms and Quick scheme [21] to the convection terms allowing one time step lag for the solid phase from the fluid phase. Implicit form of the discretized equations was solved numerically by making use of the Gauss–Seidel method. Hot and cold side boundary conditions were set as follows. In a half cycle when the fluid flows into the porous insert from the hot side, fluid non-dimensional temperature was assumed to be unity at the inlet. In another half cycle when flow is reversed in direction, fluid entering the cold side was assigned to have zero non-dimensional temperature. Fluid temperature was assumed to have zero gradient at any instant at the downstream side boundary. Along the tube axis, axisymmetry of the temperature field was assumed both for fluid and solid phases. Thus,

$$\left.\frac{\partial\theta_f}{\partial r}\right|_{r=0} = 0, \quad \left.\frac{\partial\theta_s}{\partial r}\right|_{r=0} = 0. \tag{20}$$

The heat flux was prescribed for the heat loss through the tube wall for fluid phase and solid phase as follows:

$$-\left.\frac{\partial\theta_f}{\partial r}\right|_{r=1} = \frac{Bi}{\lambda}\left(\theta_f|_{r=1} - \theta_\infty\right), \tag{21}$$

$$-\left.\frac{\partial\theta_s}{\partial r}\right|_{r=1} = Bi\left(\theta_s|_{r=1} - \theta_\infty\right). \tag{22}$$

Here Bi is the apparent Biot number, θ_∞ the ambient temperature set equal to θ_H $(= 1)$ and λ the fluid-to-solid thermal conductivity ratio. In the present study, no heat loss to the ambient, i.e., $Bi = 0$, was assumed except for a limited number of cases where $Bi = 3 \times 10^{-3}$ was assumed. The exceptional studies were just made to see the qualitative effect of the heat leakage from the ambient. So a specific value of Bi was not important. The effect was not noticeable when Bi was much smaller than the above value. Computation was started with uniformly distributed non-dimensional temperature of zero values. Solution for temperature field initially shows transient behavior from one cycle to another. Compu-

tation was carried out over 10^4 cycles. This was quite long enough for the temperature field to reach an asymptotic dynamic steady state for almost all the studied cases. In some computations for high frequency condition, cycle-to-cycle change of the computed results was very slow and asymptotic state was not attained perfectly even with the computation over the above cycles. Temperature should uniformly distribute along the radial direction when heat losses to the ambient is ignored. Therefore, a coarse grid spacing of $0.1R$ was found to be adequate. Time step was set to be equal to 1% of the oscillation period of the basic harmonic.

3.2. Characteristic values of mesh parameters

Parameters of the mesh reported in [7] or its equivalent porous insert are as follows: porosity $\varepsilon = 0.703$; wire diameter $d_w = 0.0508$ mm; mesh hydraulic diameter $d_h = 0.1205$ mm; tube radius $R = 9.5$ mm; pore surface area parameter $A_{IF} = 222.16$ [1/m]. The relationship for the measured friction factor under steady flow conditions is then expressed as follows:

$$-\varepsilon^2 \frac{dp}{dz}\frac{d_h}{R} = \frac{174.1\varepsilon}{Re_R}\frac{R}{d_h} + 2.645. \tag{23}$$

Integrated form of Eq. (2) can be written in the following form after some manipulation:

$$-\varepsilon^2 \frac{dp}{dz}\frac{d_h}{R} = \frac{2\varepsilon^3}{Re_R Da}\frac{d_h}{R} + \frac{2F_\varepsilon \varepsilon^2}{\sqrt{Da}}\frac{d_h}{R}. \tag{24}$$

A comparison of the above two relationships gives the equivalent permeability $K = 1.172 \times 10^{-10}$ m^2, and the equivalent Darcy number $Da = 1.298 \times 10^{-6}$. Further, the inertia factor has been correlated to be $F_\varepsilon = 0.24$ by using Eq. (24). Changing the length scale from the hydraulic diameter to the tube radius, the solid-to-fluid heat transfer result of [7] can be transformed into the following form:

$$Nu_R = 3.47 Re_R^{0.548}. \tag{25}$$

The mesh parameters reported in [15] can be summarized as $\varepsilon = 0.85$, $d_w = 0.2$ mm, mesh hydraulic diameter $d_h = 1.133$ mm, $R = 5$ mm, and then the equivalent values of permeability and Darcy number are $K = 6.99 \times 10^{-9}$ m^2 and $Da = 3.0 \times 10^{-4}$. The experimentally determined inertia coefficient is given by $F_\varepsilon = 0.05$. No relationship has been reported for the solid-to-fluid Nusselt number but the relationship established for a single cylinder can be used since the porosity of the mesh used in this study is quite high [22]. Applying the expressions developed for the porous media composed of spherical solid bodies [14], effective thermal conductivity of the mesh normalized with solid phase thermal conductivity can be given by the following relationships:

$$\Gamma_z = \varepsilon + 0.1 PrRe_w, \tag{26}$$

$$\Gamma_r = \varepsilon + 0.05 PrRe_w, \tag{27}$$

where Pr is the fluid Prandtl number and Re_w is the Reynolds number based on the wire diameter. This expression includes the effect of heat dispersion in fluid phase. Account was taken of the fact that the ratios of heat capacity and thermal conductivity between fluid and the mesh material i.e. phosphor–bronze were $\beta = 4 \times 10^{-4}$ and $\lambda = 3 \times 10^{-4}$. An important parameter describing the thermal performance of regenerators is a thermal time constant of the mesh wire, τ_c, defined as follows:

$$\frac{\alpha_f \tau_c}{d_w^2} = \frac{1}{\beta Nu_w} \tag{28}$$

or in another non-dimensional form

$$\frac{W\tau_c}{R} = \frac{d_w}{R}\frac{PrRe_R}{\beta Nu_R}. \tag{29}$$

Non-dimensional characteristic frequency of the mesh can then be defined as

$$\omega_c = \frac{\pi}{\tau_c}. \tag{30}$$

The values of $R\omega_c/W$ are 0.177 and 0.021 for the mesh of [7] and 0.0157 and 0.00113 for the mesh of [15], respectively, at the Reynolds number $Re_R = 100$ and 10 000.

4. Results and discussions

4.1. Flow characteristics under dynamic steady state

Time trace of velocity was sampled at two radial positions, one on axis $r = 0$ and another very near the wall $r = 0.975$, for three cases. Reynolds number and forcing frequency were assumed to be 1000 and 100. The sampled results are shown in Fig. 2. Fig. 2(a) is for the case equivalent to the mesh of [7] having uniform porosity, Fig. 2(b) is for a similar mesh but with non-uniformity of porosity and Fig. 2(c) for the case equivalent to the mesh of [15]. In Fig. 2(a), it is observed that velocity varies almost sinusoidally with time and that pattern of velocity change does not depend on the position. Sinusoidal form of velocity time trace comes from the fundamental mode of flow oscillation and suggests minor contribution from higher order modes. These match very well with the observations made in [7]. In order to have a basic idea on the effects of non-uniformity of porosity, a study was made for the case where maximum porosity at the wall is 0.85 and non-uniformity spans only over ten wire diameters with the

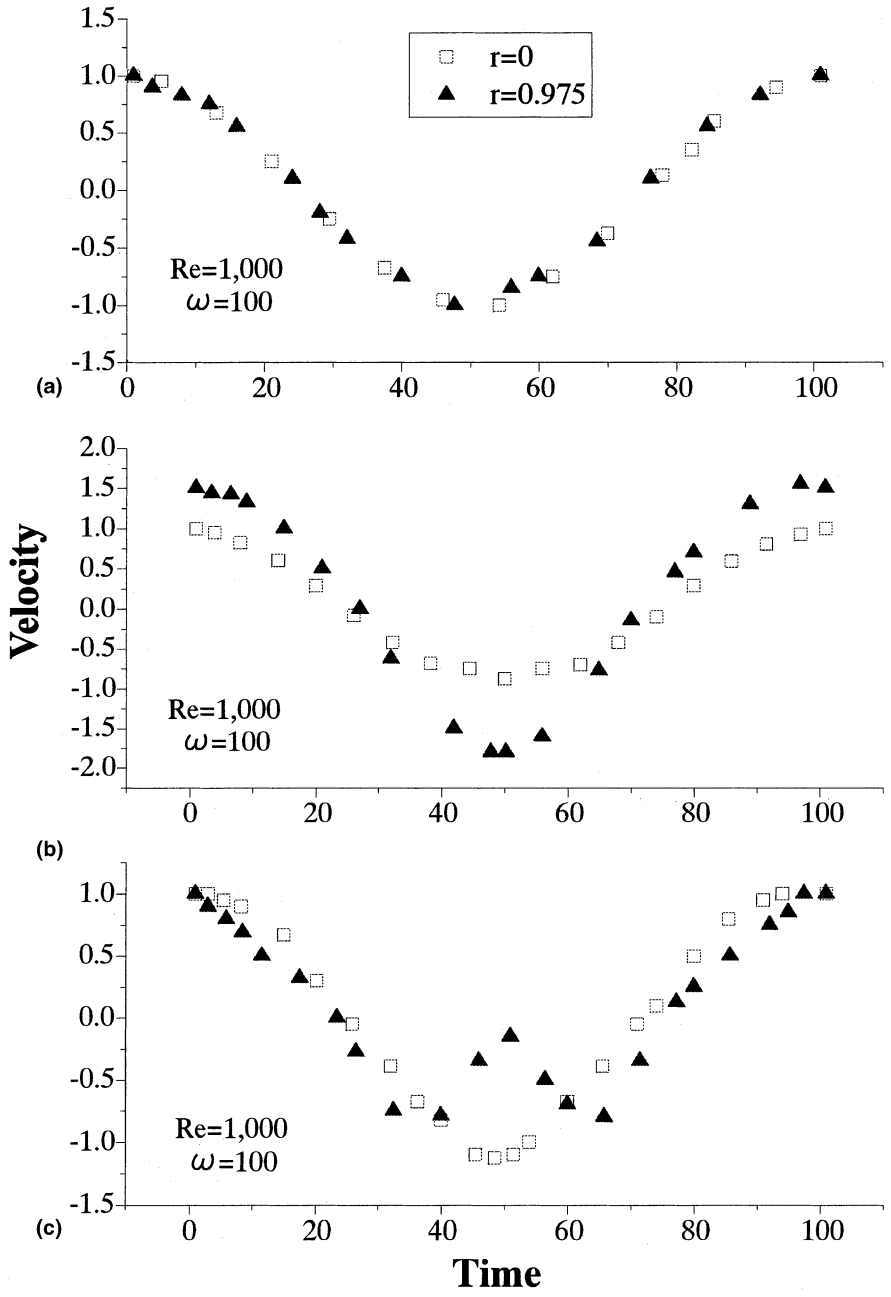

Fig. 2. Velocity time traces at two locations in the regenerator: $Re = 1000$, $\omega = 100$.

following form of porosity variation similar to the one for a packed bed of spherical particles.

$$\varepsilon(y) = \varepsilon_0\left\{1 + A_2 \exp\left[-A_1(1-r)\frac{R}{d_w}\right]\right\}, \tag{31}$$

where A_1 and A_2 were set equal to 0.304 and 0.209, respectively, with which the calculated steady flow pressure drop fits the experimental counterparts. In Fig. 2(b), velocity is observed to change with larger amplitude near the wall since higher porosity was assumed there. However, velocity varies still in an almost sinusoidal manner. Velocity change near the wall plotted in Fig. 2(c) shows significant contribution from higher order harmonics. Flow instability leading to the production of higher order harmonics occurs in this case because of high porosity of the mesh used in [15]. In the

three cases just discussed, friction factors were calculated for several conditions of different Reynolds numbers and frequencies. The obtained results are tabulated in Tables 1–3. Friction factor obtained for the jth harmonic, f_j, is equal to P_j and Real(j) and Imag(j) denote, respectively, the real and imaginary parts of P_j. Total equivalent friction factor shown in the last column is defined as follows:

$$f_{\mathrm{eq}} = \sqrt{\sum_{j=1}^{4} |P_j|^2}. \tag{32}$$

In all the studied cases of $Re = 100$, the leading harmonic dominantly contributes to the value of f_{eq}. The magnitude of imaginary part increases with an increase in frequency. However, it is much smaller than the real part so that the pressure gradient fluctuates in phase with velocity. At the Reynolds number of 10 000, the situation becomes quite different. For the uniform mesh of [7], the second harmonic gives the largest contribution to f_{eq}. In other two cases of Reynolds number of 10 000, the fourth harmonic contributes most significantly to f_{eq}. First, this means that higher order harmonics should be included for an accurate assessment of friction factor in such cases. Secondly, it indicates that flow instability is more likely to be introduced with the mesh of higher porosity or that larger pressure drop penalty has to be paid. Thus, highly porous mesh is not suitable for use in regenerators. Some basic features of the obtained results, especially the ones for P_1, can be explained based on the momentum equation. In the core region inside the porous insert, velocity or ϕ_1 distributes

Table 1
Friction factor as a function of Reynolds number and frequency (mesh of [7])

ω	Real(1)	Imag(1)	Real(2)	Imag(2)	Real(3)	Imag(3)	Real(4)	Imag(4)	f_{eq}
$Re = 100$									
1	0.77E + 4	0.25	0.21E + 3	0	−0.69E − 2	0	0	0	0.733E + 4
10	0.77E + 4	0.25E + 1	0.21E + 3	0	−0.69E − 2	0	0	0	0.773E + 4
100	0.77E + 4	0.25E + 2	0.21E + 3	0	−0.69E − 2	0	0	0	0.773E + 4
1000	0.77E + 4	0.25E + 3	0.21E + 3	−0.9E − 2	−0.7E − 2	0	0	0	0.773E + 4
$Re = 10000$									
1	0.77E + 2	0.3E − 1	0.21E + 3	0	−0.7	0	0.26E + 1	−0.6E − 2	0.225E + 3
10	0.77E + 2	0.3	0.21E + 3	−0.11E − 2	−0.69	0.92E − 2	0.26E + 1	−0.59E − 1	0.225E + 3
100	0.77E + 2	0.31E + 1	0.21E + 3	−0.1E − 1	−0.68	0.92E − 1	0.26E + 1	−0.58	0.225E + 3
1000	0.77E + 2	0.31E + 2	0.21E + 3	−0.89E − 1	−0.35	0.44	0.11E + 1	−0.18E + 1	0.227E + 3

Table 2
Friction factor as a function of Reynolds number and frequency – effect of variable porosity (mesh of [7])

ω	Real(1)	Imag(1)	Real(2)	Imag(2)	Real(3)	Imag(3)	Real(4)	Imag(4)	f_{eq}
$Re = 100$									
1	0.79E + 4	0.27	0.25E + 3	−0.8E − 2	−0.75E + 1	0.33E − 2	0.18E + 1	−0.13E − 2	0.796E + 4
10	0.79E + 4	0.27E + 1	0.25E + 3	−0.8E − 1	−0.75E + 1	0.33E − 1	0.18E + 1	−0.13E − 1	0.796E + 4
100	0.79E + 4	0.27E + 2	0.25E + 3	−0.8	−0.75E + 1	0.33	0.18E + 1	−0.13	0.796E + 4
1000	0.79E + 4	0.27E + 3	0.25E + 3	−0.78E + 1	−0.65E + 1	0.30E + 1	0.13E + 1	−0.11E + 1	0.796E + 4
$Re = 10000$									
1	0.79E + 2	0.3E − 1	0.25E + 3	−0.98E − 1	−0.75E + 3	0.41E + 1	0.18E + 5	−0.17E + 3	0.27E + 5

Table 3
Friction factor as a function of Reynolds number and frequency (mesh of [15])

ω	Real(1)	Imag(1)	Real(2)	Imag(2)	Real(3)	Imag(3)	Real(4)	Imag(4)	f_{eq}
$Re = 100$									
1	0.34E + 2	0.19E − 1	0.30E + 1	0	−0.6E − 2	0	0.55E − 3	0	0.34E + 2
10	0.34E + 2	0.19	0.30E + 1	−0.48E − 3	−0.6E − 2	0	0.55E − 3	0	0.34E + 2
100	0.34E + 2	0.19E + 1	0.30E + 1	−0.48E − 2	−0.6E − 2	0.85E − 3	0.55E − 3	−0.16E − 3	0.35E + 2
1000	0.34E + 2	0.75E + 1	0.30E + 1	−0.18E − 1	−0.46E − 2	0.27E − 2	0.21E − 3	−0.38E − 3	0.35E + 2
$Re = 10000$									
1	0.346	0.13E − 2	0.30E + 1	−0.35E − 3	−0.61	0.62E − 2	0.55E + 1	−0.12	0.63E + 1

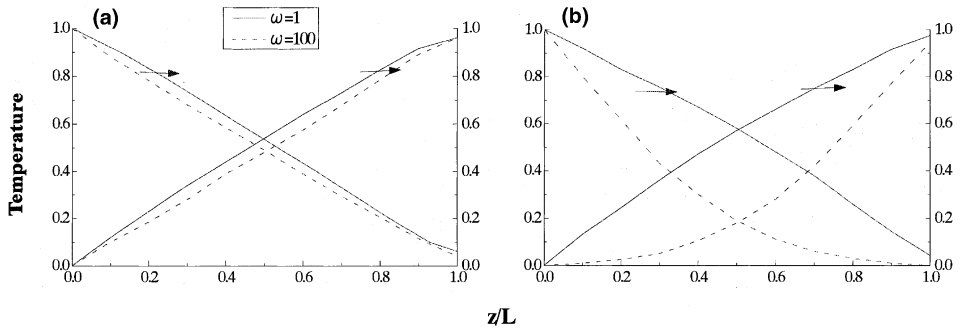

Fig. 3. Temperature profile along the axis of the regenerator: (a) $Re = 10000$, $L = 5$; (b) $Re = 10000$, $L = 10$ (mesh of Chen–Chang–Huang).

uniformly at any instant and takes almost the real number close to unity in the cases tabulated in Table 1. Therefore, Eq. (9) reads approximately as

$$\frac{i\omega}{\varepsilon}\phi_1 = P_1 - \frac{1}{Re_R Da}\phi_1. \tag{33}$$

Thus, the real part of friction factor should be reciprocally proportional to Re and on the other hand its imaginary part should be proportional to the forcing frequency ω.

4.2. Thermal performance

Some examples of instantaneous temperature distributions inside the porous insert equivalent to the mesh used in [7] are shown in Fig. 3. Fig. 3(a) is for the $5R$ long insert and Fig. 3(b) for the $10R$ long one. In both the figures, two lines sloping right-side down show the maximum temperatures to be attained in a hot flow phase, i.e., in the phase when hot gas flows into the insert at its hot end. The other two lines sloping up to the right show the minimum temperatures to be attained in a cold flow phase, namely in the phase when cold flow flows back into the insert through its cold end. Abscissa of these figures is the distance from the hot end or from the cold end of the respective phases. At the hot end, both solid and fluid are of the temperature 1.0 in a hot flow phase and temperature is zero both for solid and fluid phases at cold end in a cold reversed flow phase. Temperature gradually changes from its end value toward another end. Outflow end temperature neither attains zero value in a hot flow phase nor unity in a cold flow phase. Thus, regenerator effectiveness defined below is smaller than the ideal value of unity.

$$E = \frac{\theta_h - \theta_L}{\theta_H - \theta_L}, \tag{34}$$

where θ_h is the outflow non-dimensional (cycle-averaged) temperature at the hot end to be attained in a cold flow phase, and θ_H and θ_L are the non-dimensional temperatures corresponding to temperatures T_H and T_L. Solid phase and fluid phase reach different temperatures from each other. Difference is larger for the longer insert but is not affected so much by frequency. Another example of instantaneous temperature distributions is shown in Fig. 4 for the insert equivalent to the mesh of [15]. In this high porosity case, discrepancy of outflow temperature from its ideal value is larger so that the regenerator effectiveness takes a smaller value. Therefore, a screen mesh of high porosity is not good for use in regenerators also from a thermal view point.

Tables 4 and 5 show the effect of frequency on regenerator effectiveness and the maximum and minimum temperatures of solid and fluid phases,

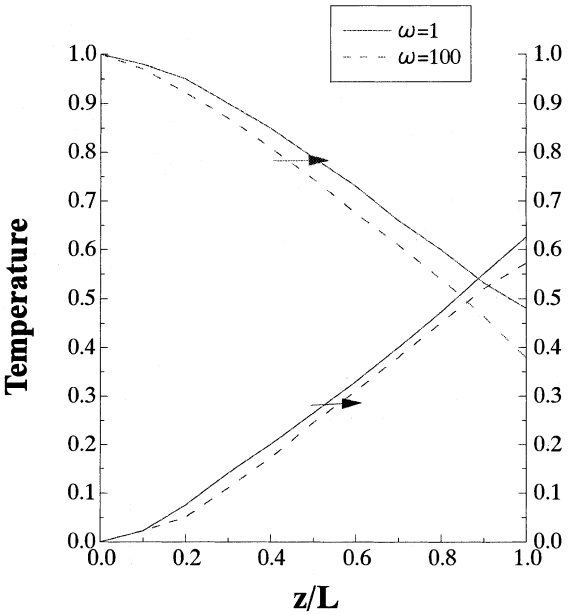

Fig. 4. Temperature profile along the axis of the regenerator: $Re = 10000$, $L = 5$ (mesh of Sozen–Kuzay).

Table 4
Regenerator effectiveness and mid-point temperature for mesh screen of [7] ($Re = 100$, $L = 5$)

ω	θ_f		θ_s		E
	max	min	max	min	
1	0.503	0.501	0.503	0.502	0.908
10	0.502	0.500	0.501	0.501	0.942
100	0.502	0.500	0.501	0.501	0.950
1000	0.214	0.213	0.213	0.213	0.932

Table 5
Regenerator effectiveness and mid-point temperature for mesh screen of [7] ($Re = 10000$, $L = 10$)

ω	θ_f		θ_s		E
	max	min	max	min	
1	0.582	0.564	0.579	0.566	0.950
10	0.577	0.566	0.573	0.571	0.953
100	0.245	0.234	0.239	0.239	0.932
1000	0.6E − 4	0.4E − 4	0.5E − 4	0.5E − 4	0.847

respectively. The porous insert treated in these computations is the one equivalent to the mesh of [7]. These tables demonstrate that there is an optimum frequency achieving the maximum regenerator effectiveness. Amplitude of temperature fluctuation is small both for fluid and solid phases. Table 6 tabulates the results for similar inserts but of different lengths. Longer insert gives larger regenerator effectiveness but improvement to be obtained by replacing $5R$ long insert by $20R$ long one is not very significant. The temperature to be attained at the middle of the insert differs very much from 0.5 for inserts of $10R$ and $20R$ lengths. It indicates that, in more than half the insert, solid phase does not effectively participate in heat exchange with the fluid phase. However, this should be judged with reservation. As will be discussed later, asymptotic dynamic steady state has not been achieved yet in these cases with the computation over 10^4 cycles. Addition of such an ineffective part is not desirable anyway because larger pressure loss penalty has to be paid with a longer insert.

Table 7 shows similar results for the case where heat loss to the ambient through the tube wall occurs. In this computation, Biot number was assumed to be 3×10^{-3}. Comparing the results with the counterparts for zero heat loss case tabulated in Table 6, it is observed that heat loss reduces the regenerator effectiveness. Table 8 shows the results for the mesh screen of [15]. As was observed in Fig. 4, it is confirmed that high porosity screen mesh takes a lower value of the regenerator effectiveness. One point noticeable in this table is that temperatures of both of fluid and solid phases fluctuate

Table 6
Regenerator effectiveness and mid-point temperature for mesh screen of [7] ($Re = 10000$)

ω	θ_f		θ_s		E
	max	min	max	min	
$L = 1$					
1	0.573	0.451	0.561	0.464	0.768
100	0.552	0.470	0.512	0.511	0.794
$L = 5$					
1	0.553	0.525	0.550	0.528	0.929
100	0.486	0.467	0.477	0.477	0.927
$L = 10$					
1	0.582	0.564	0.579	0.566	0.950
100	0.245	0.234	0.239	0.239	0.932
$L = 20$					
1	0.648	0.641	0.648	0.642	0.963
100	0.7E − 2	0.6E − 2	0.7E − 2	0.7E − 2	0.928

Table 7
Regenerator effectiveness and mid-point temperature for mesh screen of [7] ($Re = 10000$, $L = 10$, $Bi = 3 \times 10^{-3}$)

ω	θ_f		θ_s		E
	max	min	max	min	
1	0.518	0.490	0.515	0.494	0.887
10	0.513	0.495	0.505	0.502	0.892
100	0.462	0.444	0.453	0.452	0.887
1000	0.2E − 1	0.2E − 1	0.2E − 1	0.2E − 1	0.805

Table 8
Regenerator effectiveness and mid-point temperature for mesh screen of [15] ($Re = 10000$, $L = 5$)

ω	θ_f		θ_s		E
	max	min	max	min	
1	0.840	0.188	0.766	0.271	0.616
100	0.746	0.268	0.514	0.508	0.669

with much larger amplitude than the ones for other cases discussed in the above.

4.3. Transient response

In Section 5, transient response of thermal field occurring after the start of computation is briefly discussed. Temperature field starts from the uniform zero-value distributions both for solid and fluid phases. After the start of computation, alternating rise and fall of temperature occur in solid phase following the alternating heating and cooling phases, i.e., heating in one half cycle with hot fluid supplied through one end and cooling in the next half cycle with cold fluid through the other end. Because of larger heat transfer rate in the heating period than in the cooling period due to larger fluid-to-solid temperature difference in the heating period, non-uniform temperature distribution gradually develops in the solid phase accompanying a certain degree of fluctuation. Similarly, non-uniform temperature distribution develops in the fluid phase too. Both distributions asymptotically approach the ones for dynamic steady state with progress of computation. Fig. 5 shows the cycle-to-cycle variations of the mid-point fluid temperature and the space mean temperature over the whole length of insert. The porous inserts adopted in this computation are equivalent to the wire mesh of [7]. All of the Reynolds number, frequency and length of insert seriously affect the transient behavior of the mid-point temperature and spatial mean temperature. Asymptotic state can be obtained in many cases within the 10 000 cycles studied. In the case of $L = 10$ and frequency being 100 for Reynolds number of 10 000, the attained state after 10 000 cycles is still far from an asymptotic one. This behavior suggests the nature of transient response of the corresponding regenerators in practical use although the temperature difference between the hot and

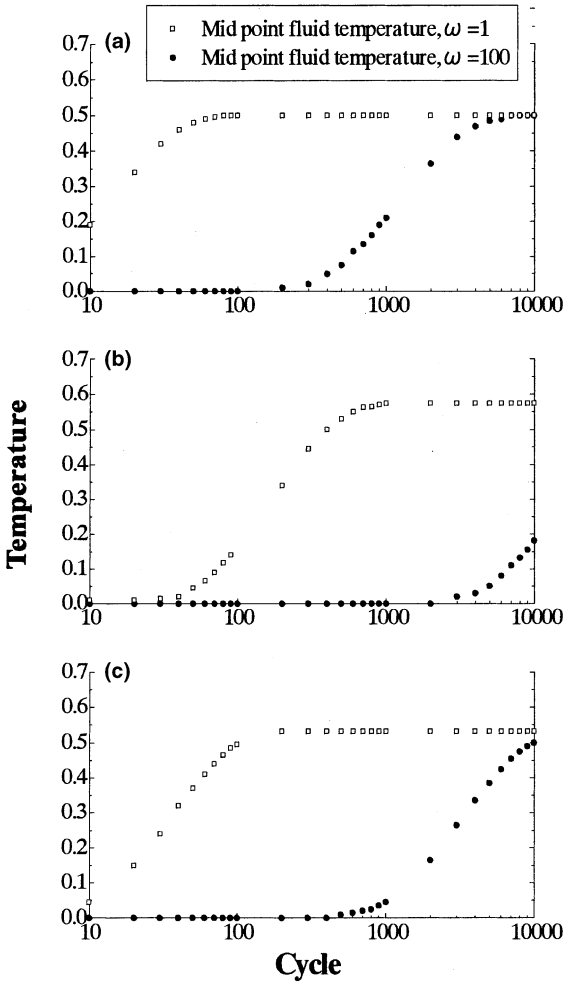

Fig. 5. Variation of mid-point fluid temperature with time: (a) $Re = 100$, $L = 10$; (b) $Re = 10000$, $L = 10$; (c) $Re = 10000$, $L = 5$ (mesh of Chen–Chang–Huang).

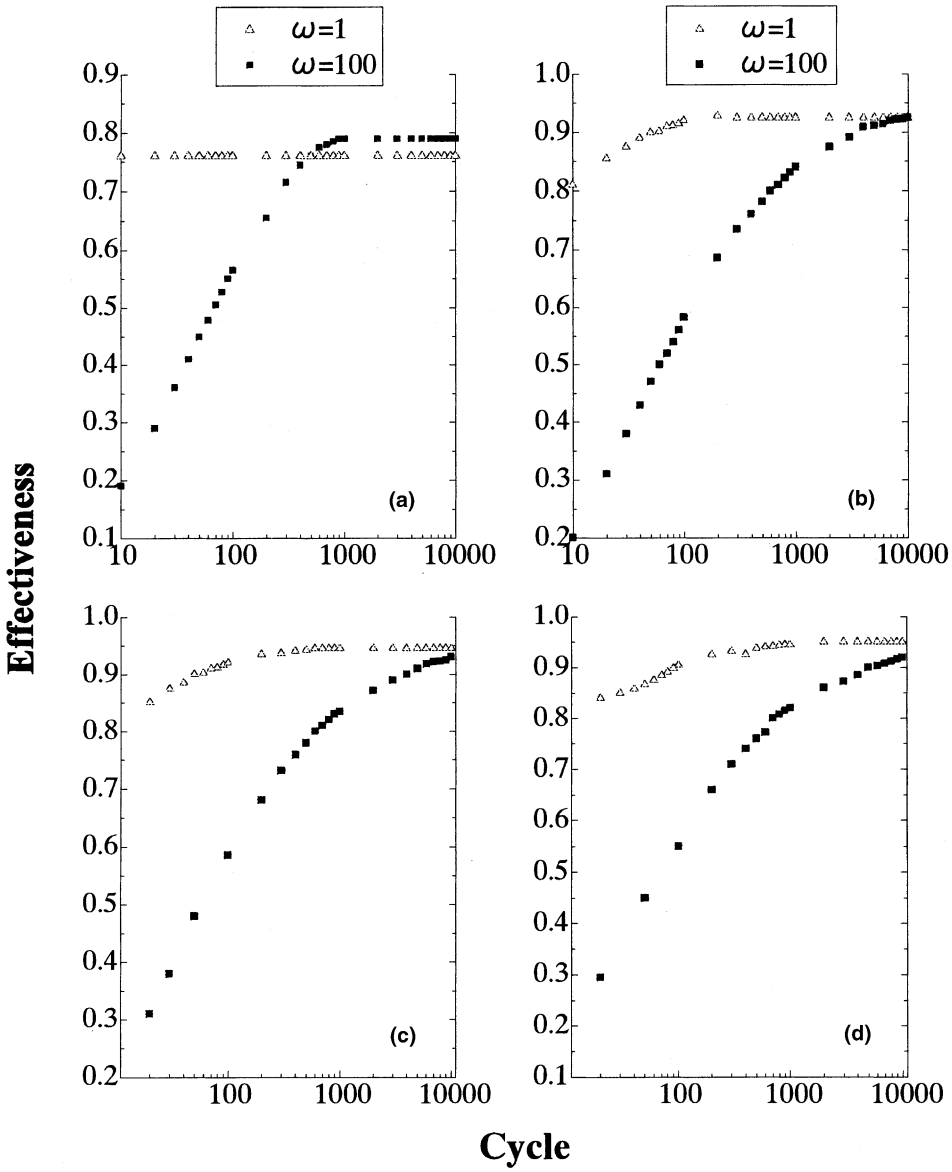

Fig. 6. Variation of effectiveness with time, $Re = 10000$: (a) $L = 1$; (b) $L = 5$; (c) $L = 10$; (d) $L = 20$ (mesh of Chen–Chang–Huang).

cold ends starts from zero in actual practice and gradually increases up to an asymptotic maximum one. Fig. 6 illustrates the transient variation of the regenerator effectiveness for the cases discussed in Fig. 5. It is observed that the regenerator effectiveness approaches its asymptotic value faster than the mid-point temperature and the spatial mean temperature just discussed above. Even in the case where the mid-point temperature attained after 10 000 cycles was found to be far from its asymptotic one in Fig. 5, regenerator effectiveness is judged to more rapidly approach its asymptotic value to be attained at the dynamic steady state.

5. Concluding remarks

Based on a model treating the mesh-screen regenerator as a porous insert and taking an idea that flow attains much more rapidly the dynamic steady state than the thermal field, a harmonic analysis technique was used in the computation of velocity field. By making use of the calculated velocity field information, axisymmetric time-dependent temperature field was further computed with a finite difference approach. The main conclusions drawn from the computation are as follows:

1. With the mesh screen of normal porosity reported in [7], velocity varies sinusoidally with time keeping spatial uniformity at any instant except in a thin region near the tube wall. In this case, pressure gradient changes in phase with velocity. With high porosity mesh screen of [15], flow instability is likely to occur and induces higher order harmonics. In this case, higher order harmonics contribute significantly to the value of effective friction factor. In the high Reynolds number range of this case, flow becomes turbulent which should be studied with a different approach.
2. At a low Reynolds number below 100, dynamic steady state can be reached for thermal field well within 10^4 cycles even at a non-dimensional frequency lower than 100. Regenerator effectiveness is as high as the value around 0.9 for the mesh screen of [7], if its length is equal to or larger than $5R$, even at the Reynolds number of 10 000. Regenerator efficiency is slightly raised by elongation of mesh screen but mesh screen longer than $5R$ is not recommended because pressure loss increase caused by the elongation of mesh screen is much more noticeable. With the high porosity mesh screen of [15], amplitude of temperature fluctuation is larger and the regenerator efficiency is lower.
3. Heat loss toward the ambient through the tube wall results in lower regenerator effectiveness. This should be studied in future and the present method is useful for the quantitative assessment of such a heat loss effect.

Acknowledgements

This work was carried out partially supported by the Grant-in-Aid for Exploratory Research #09875060 of the Ministry of Education, Science, Sports and Culture, Japan during his stay with one of the authors (KM) at the Kyoto University as a fellow of the Japan Society for Promotion of Science.

References

[1] G. Walker, Cryocoolers, Part 1 and 2, International Cryogenics Monographs Series, Plenum Press, New York, 1983.
[2] J.G. Brisson, G.W. Swift, Measurements and modelling of recuperator for superfluid Stirling refrigerator, Cryogenics 34 (1994) 971–982.
[3] T.M. Kuzay, J.T. Collins, A.M. Khounsary, G. Morales, Enhanced heat transfer with metal wool-filled tubes, in: Proceedings of the ASME/JSME Thermal Engineering Conference, 1991, pp. 145–151.
[4] M.D. Atrey, D. Heiden, Performance evaluation of an optimized two-stage, free displacer plastic Stirling cryocooler with gap regenerator, Cryogenics 36 (1996) 47–52.
[5] L. Bauwens, Stirling cryocooler model with stratified cylinders and quasi-steady heat exchangers, J. Thermophys. Heat Transfer 9 (1995) 129–135.
[6] X.Z. Tang, H. Yoshida, J.H. Yun, R. Echigo, Numerical analysis of unsteady heat transfer characteristics of a stirling engine regenerator, Trans. JSME B 56–525 (1990) 1440–1447.
[7] P.H. Chen, Z.C. Chang, B.J. Huang, Effect of oversize in wire-screen matrix to the matrix-holding tube on regenerator thermal performance, Cryogenics 36 (1996) 365–372.
[8] S. Isshiki, A. Sakano, I. Ushiyama, N. Isshiki, Studies on flow resistance and heat transfer of regenerator wire meshes of Stirling engines in oscillatory flow, Trans. JSME B 62–604 (1996) 4254–4261.
[9] M. Kaviany, Principles of Heat Transfer in Porous Media, Mechanical Engineering Series, Springer, New York, 1991.
[10] K. Vafai, S.J. Kim, Forced convection in a channel filled with a porous medium: an exact solution, Trans. ASME J. Heat Transfer 111 (1989) 1103–1106.
[11] G. Lauriat, V. Prasad, Non-Darcian effects on natural convection in a vertical porous enclosure, Int. J. Heat Mass Transfer 32 (1989) 2135–2148.
[12] J.L. Lage, On the theoretical prediction of transient heat transfer within a rectangular fluid-saturated porous medium enclosure, Trans. ASME J. Heat Transfer 115 (1993) 1069–1071.
[13] B.V. Antohe, J.L. Lage, Amplitude effect on convection induced by time-periodic horizontal heating, Int. J. Heat Mass Transfer 39 (1996) 1121–1133.
[14] A. Amiri, K. Vafai, Analysis of dispersion effects and non-thermal equilibrium, non-Darcian, variable porosity incompressible flow through porous media, Int. J. Heat Mass Transfer 37 (1994) 939–954.
[15] M. Sozen, T.M. Kuzay, Enhanced heat transfer in round tubes with porous inserts, Int. J. Heat Fluid Flow 17 (1996) 124–129.
[16] S.Y. Kim, B.H. Kang, J.M. Hyun, Heat transfer from pulsating flow in a channel filled with porous media, Int. J. Heat Mass Transfer 37 (1994) 2025–2033.
[17] A.V. Kuznetsov, An investigation of a wave of temperature difference between solid and fluid phases in a porous media, Int. J. Heat Mass Transfer 37 (1994) 3030–3033.
[18] A.V. Kuznetsov, A perturbation solution for a nonthermal equilibrium fluid flow through a three dimensional sensible storage packed bed, Trans. ASME J. Heat Transfer 118 (1996) 508–510.
[19] A.V. Kuznetsov, K. Vafai, Analytical comparison and criteria for heat and mass transfer models in metal hydride packed beds, Int. J. Heat Mass Transfer 38 (1995) 2873–2884.
[20] K. Vafai, M. Sozen, Analysis of energy and momentum transport for fluid flow through a porous bed, Trans. ASME J. Heat Transfer 112 (1990) 690–699.
[21] B.P. Leonard, A stable and accurate convective modelling procedure based on quadratic upstream interpolation, Comput. Methods Appl. Mech. Eng. 19 (1979) 59–98.
[22] M.N. Ozisik, Heat Transfer: A Basic Approach, McGraw-Hill, New York, 1985.